Journal of Structural Geology 30 (2008) 929–945

Contents lists available at ScienceDirect

Journal of Structural Geology

journal homepage: www.elsevier.com/locate/jsg

Three-dimensional seismo-tectonic imaging: An example from the Southern California Transverse Ranges

Peter A. Geiser [a,*], Leonardo Seeber [b]

[a] STRM, LLC, 1435 Yarmouth, Suite 106, Boulder, CO 80304, USA
[b] Lamont Doherty Earth Observatory, Palisades, NY, USA

ARTICLE INFO

Article history:
Received 10 June 2005
Received in revised form 6 February 2008
Accepted 8 February 2008
Available online 4 March 2008

Keywords:
Structural geology
Seismology
California Transverse Range

ABSTRACT

We present a new technique to image deformation, 3D seismo-tectonic imaging, which juxtaposes instantaneous and accumulated deformation by combining earthquake and structural geology data. We test the technique using three independent data sets. We find concordance between the predicted finite deformation field and related instantaneous deformation surfaces inferred from aftershock and background seismicity data as well as structure imaged by seismic reflection data. These results indicate that:

[1] The 1994 Northridge event ruptured a transverse, high-angle reverse fault linking two EW striking listric thrust systems, the Pico and Oak Ridge. The rupture terminated on the thrusts and was capped by a north dipping, forward-breaking imbricate of the Santa Susana Fault.
[2] The Los Angeles Seismic Zone is a region of thrusting associated with the development of a new mountain front forming south of the present one represented by the Santa Monica Anticline. The thrust is rooted on a mid-crustal ramp forming beneath the Los Angeles basin.

We conclude that seismo-tectonic imaging by linking earthquake data to an empirically based quantitative description of the finite deformation field provides a new and fruitful method for integrating geological and seismological data.

1. Introduction

In this paper we explore the relationship between seismogenesis as an instantaneous incremental strain and structure as finite strain. We use classical structural analysis (e.g. Suppe, 1983; Davis et al., 1989; Geiser, 1988), but incorporate a dense field of focal mechanisms from small earthquakes. We define this approach as seismo-tectonic imaging (STI) that discriminates between active seismogenic structures, which contribute to the current deformation regime and passive or pre-existing structures that are not involved in the current regime. Thus seismo-tectonic imaging addresses issues at the intersection of structural geology and seismogenesis, such as whether the timing for deformation during the cycle of large earthquakes differs for different elements in the system.

Earthquake slip planes provide information about locations and kinematic interactions of faults. Further, because micro-seismicity has the potential of illuminating tectonic elements below the resolution of either seismic reflection or structural data (i.e. 10–100 m scale e.g. Rutledge et al., 1994), the dense data from small earthquakes provide an ideal link between seismological observations and fault systems as depicted from geologic data. Thus, earthquake data can complement geologic data for exposed as well as hidden structures in terms of both their seismogenic behavior and structural linkage.

We construct a three-dimensional transect through the Northridge area of the Transverse Ranges (Fig. 1) where recent seismic sequences provide hundreds of reliable focal mechanisms of small earthquakes allowing consideration of the following:

- Is the seismicity consistent with patterns of finite strain?
- Which structures are seismogenic?
- Do earthquakes and structure provide complementary data for resolving rock deformation patterns?
- Can one data set be used to test the other where they overlap?

Because the two data sets (structural and earthquake) are independent, initial analysis of the data is done "blind", i.e. the earthquake and structural analysis are done separately and then input to a 3D section construction program (e.g. Geosec 3D) both as

* Corresponding author. Tel.: +1 303 443 2920.
E-mail address: pete@strmllc.com (P.A. Geiser).

0191-8141/$ – see front matter © 2008 Elsevier Ltd. All rights reserved.
doi:10.1016/j.jsg.2008.02.010

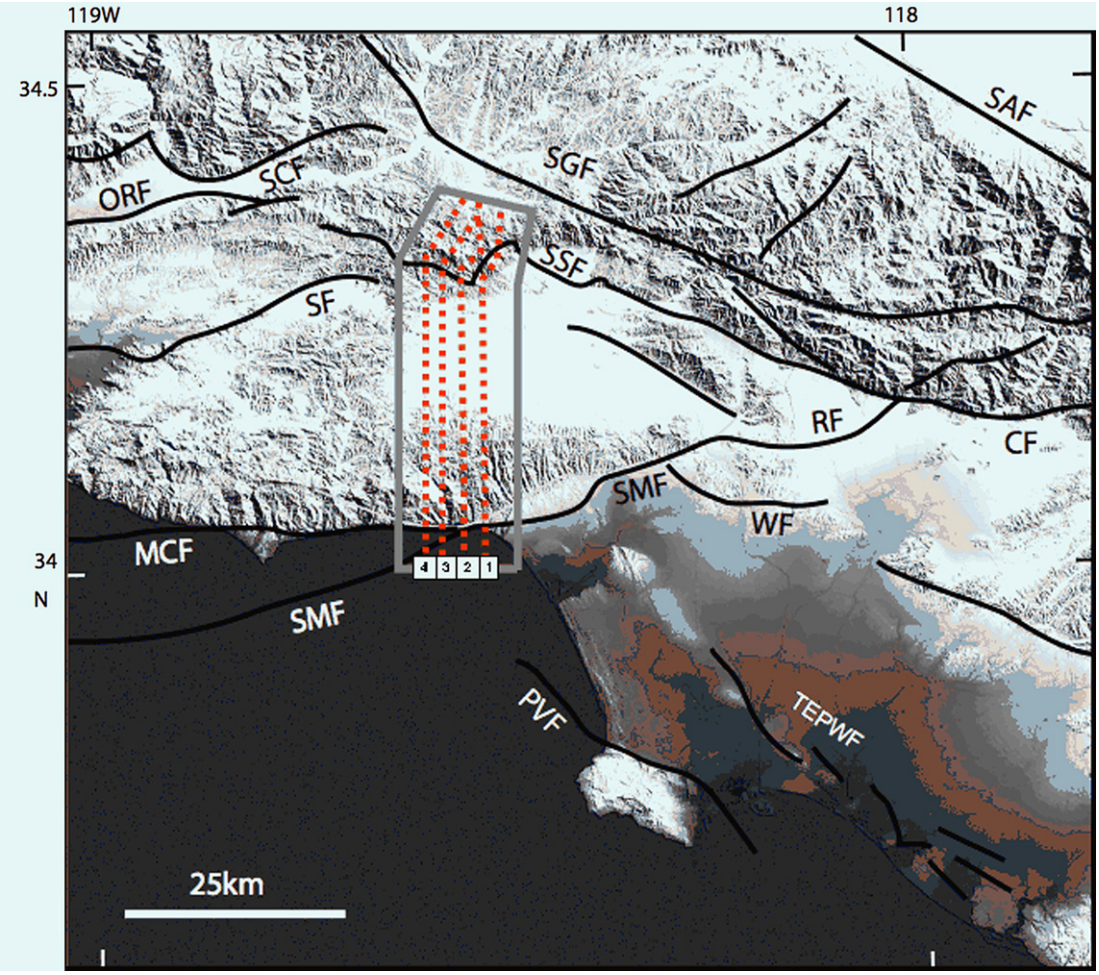

Fig. 1. Study area with inset map showing locations of serial sections used in constructing 3D model. SAF, San Andreas Fault; SGF, San Gabriel Fault; SCF, San Cayetano Fault; SSF, Santa Susana Fault; ORF, Oak Ridge Fault; SF, Simi Fault; RF, Raymond Fault; MCF, Malibu Coast Fault; SMF, Santa Monica Fault; CF, Cucamonga Fault; WF, Whittier Fault; TEPWF, Torrance, Elysian Park, Wilmington Faults; PVF, Palos Verdes Fault. The Los Angeles Basin is the area south of the SMF.

independent checks and to form a consistent model. The focus of this paper is on the analysis of the first-order structures (20 km wavelength) of the Transverse Ranges.

2. Three-dimensional seismo-tectonic imaging

2.1. Earthquakes as structural data

In a seismogenic upper crust over a short time period, a fault network may host a few intermediate to large earthquakes but is better imaged by the more abundant micro-seismicity. Phase data from dense seismic networks, such as southern California, provide focal mechanisms for this "background" activity.

One of us (Seeber) constructed a structural model of seismicity for southern California (e.g. Seeber and Armbruster, 1995) based on a large focal mechanism data set obtained from Caltech–USGS network. Hypocenters were calculated from a set of location-dependent travel-time corrections for each of the station optimizing the accuracy of locations relative to each other. This is particularly important when interpreting fault-rupture planes from nodal planes based on hypocenter distribution. Focal mechanisms were obtained by a grid-search procedure that optimizes the fit of a double-couple source to the first motions. The procedure also yields several quality factors for both locations and focal mechanisms, which can be applied interactively during the interpretation to explore the trade-off between data density and quality. This maximizes information on fault kinematics. In the area of this study, we find that scatter of hypocenters about inferred fault planes is typically ± 0.5 km, reflecting location uncertainty of the horizontal component. Hypocenters significantly farther than 1 km apart normal to the hypothesized fault plane are usually assumed to originate from different faults. Both for reasons of station geometry (there are fewer instruments at high angles to the wave front for shallower events than deeper ones) and the higher variability of velocities in the shallow crust, vertical uncertainty may be larger, particularly for events in the shallowest part of the seismogenic zone.

The 3D visualization and categorization procedure greatly facilitates the interpretation of the mechanisms in terms of "slip planes", the nodal planes inferred to indicate the seismogenic fault. The reliability of the interpretations from this procedure would normally be difficult to assess; however, the innovation of the simultaneous use of a large number of focal mechanisms improves reliability (e.g. Seeber and Armbruster, 2000). In this approach the simultaneous use of large numbers of focal mechanisms allows the systematic comparison between hypocenter distribution and attitude of nodal planes for structural interpretation (see Seeber and Armbruster, 2000, for details). These data provide a wealth of internal reliability checks. Fig. 2 shows the representative distribution of the 3004 slip planes used in the study. This represent about 80% of the available data at the selected level of confidence ($xy = 250$ m; $yz = 500$ m; NB: these relative value error estimates

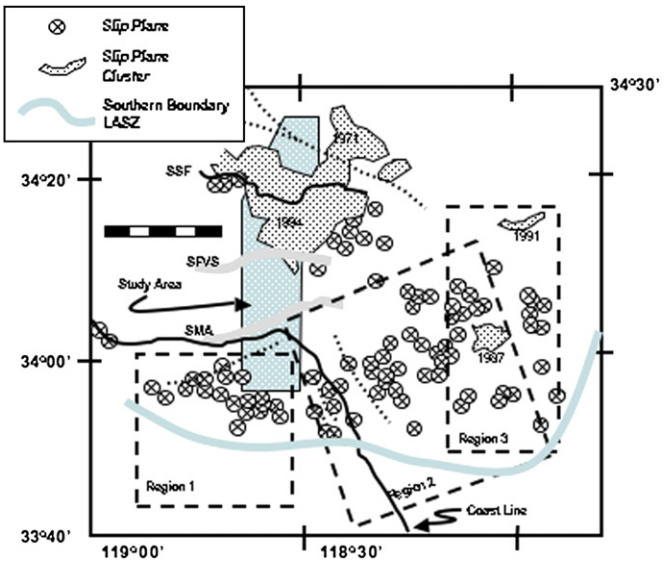

Fig. 2. Location of earthquake data used in study. Stippled areas locate aftershock clusters of dated events. Epicentral locations shown for "background" seismicity; 1971 = San Fernando Valley earthquake, 1987 = Whittier earthquake, 1991 = Sierra Madre, 1994 = Northridge earthquake (see Fig. 6 for view of this data set). SSF = Santa Susana Fault; SFVS = San Fernando Valley Synclinorium; SMA = Santa Monica Anticlinorium; LASZ = Los Angeles Seismic zone. Regions 1–3 were selected to show the hypocenter geometry by projection to a vertical plane located in the center of each region (see Fig. 4).

may be underestimates; Armbruster and Seeber, SCEC data center: http://www.data.scec.org/ftp/focal/focal1.nano). Of the 3004 slip planes used our detailed kinematic analysis focuses on the 2047 slip planes that intersect the region controlled by our serial geologic sections (see Fig. 1 and Table 1).

2.2. Linked slip systems

During deformation rock volumes must maintain physical compatibility. This requirement can be considered in terms of two elements: *internal kinematic* surfaces and *external kinematic* surfaces. Note that these are abstract elements subjected to mathematical analysis (e.g. Ramsay, 1967; Suppe, 1983). In contractional regimes, a useful first-order description of the geometric and kinematic behavior of rock deformation is the layer-parallel flexural-slip/flow model (e.g. Suppe, 1983; Geiser et al., 1988). In this model, the directions of finite simple shear parallel the directions of no finite longitudinal strain (e.g. Ramsay, 1967, p. 463). In turn these directions are controlled by the external geometric boundary conditions in terms of wavelength/thickness ratios rather than layer anisotropy (e.g. Ramberg, 1961; Keunen and De Sitter, 1938; Geiser, 1970).

Using this condition, applicable to the contractional system of the Transverse Range (e.g. Davis and Namson, 1994) and following Ramsay's (1967) flexural-slip description, we define our surfaces as shown in Fig. 3.

- *Internal kinematic surfaces* are defined by the directions of no finite longitudinal strain that parallel the directions of finite simple shear. Although these are kinematic rather than bedding surfaces they conform to fold and fault geometry.
- *External kinematic surfaces* (*mnp*) are physical boundaries that either terminate or bound the internal kinematic surfaces. Examples of external kinematic surface are faults associated with fault-propagation folds (*mnp*, Fig. 3) or surfaces across which mechanically significant viscosity contrasts occur.

Table 1
Earthquake data used for seismo-tectonic imaging

Earthquake data set name	Number of events
Los Angeles Seismic Zone [LASZ]	195
1994 Northridge main-shock	386
1994 Northridge Terminations	805
Santa Susana Fault [set 14]	603
Pico Forelimb [set 18]	58

The internal and external kinematic surfaces are kinematically linked, i.e. movement of one set requires movement of the other. An additional possible strain component is any imposed "global" simple shear (Geiser, 1988) illustrated by the simple shear profile of Fig. 3 and reflected in the shape of the deformed state loose line, *om*, initially perpendicular to the simple shear directions.

Fig. 3 shows two aspects of the deformation model that can be used to infer the locations of foci and their characteristics:

- The distribution of the kinematic surface(s): the *external deformation fields* are defined by Slip Systems that bound the deformed rock, e.g. the bounding faults of a horse. The *internal deformation fields* are defined by the suite of active slip surfaces ranging from grain boundaries to small displacement faults that form the Internal Slip System bounded by the External Slip System.
- The finite structural geometry: the structural geometry defines fold domains and fault positions.

The first characteristic suggests that clouds of earthquake slip planes with systematic orientation and kinematics illuminate the Internal Slip System. For example, scale dependent statistical analysis of the slip directions (Marshak et al., 1982) using slip data from fractures at the 10–100 cm scale in folds with wavelengths at the 100 m scale gives the orientations of the finite simple shear directions defining the internal deformation field. The bounding surfaces of the data cloud are the External Slip System that consists of the faults bounding the internal deformation field (e.g. floor and roof thrusts, etc.; compare Figs. 3 and 4).

2.3. Analysis of earthquake data

2.3.1. Seismicity

Most slip planes in Fig. 2 are concentrated in dense aftershock zones (e.g. 1971, 1987, 1991, 1994). Aftershocks from the main rupture not only reflect the main-shock kinematics, but also illuminate a number of related faults that may be the sources of future large earthquakes. For example, following the 1971 San Fernando

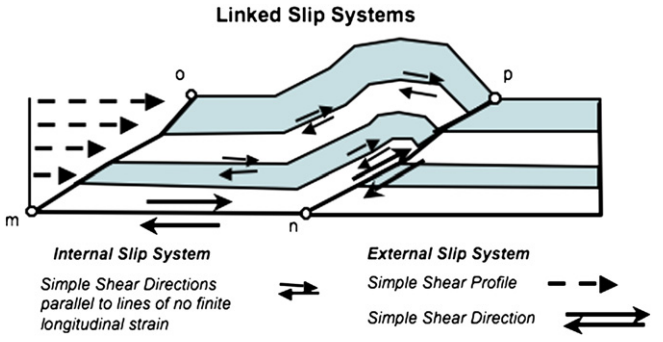

Fig. 3. Fault-propagation fold illustrating "linked slip systems" concept whereby motion on fault *mnp* requires deformation of hanging wall. Note that distributed deformation of the hanging wall contrasts with the localized slip on fault *mnp*. We infer that the distributed deformation of the Internal Slip System is expressed as a slip plane "cloud" whereas the localized slip of the External Slip System boundary *mnp* is the fault forming the lower boundary of the "cloud".

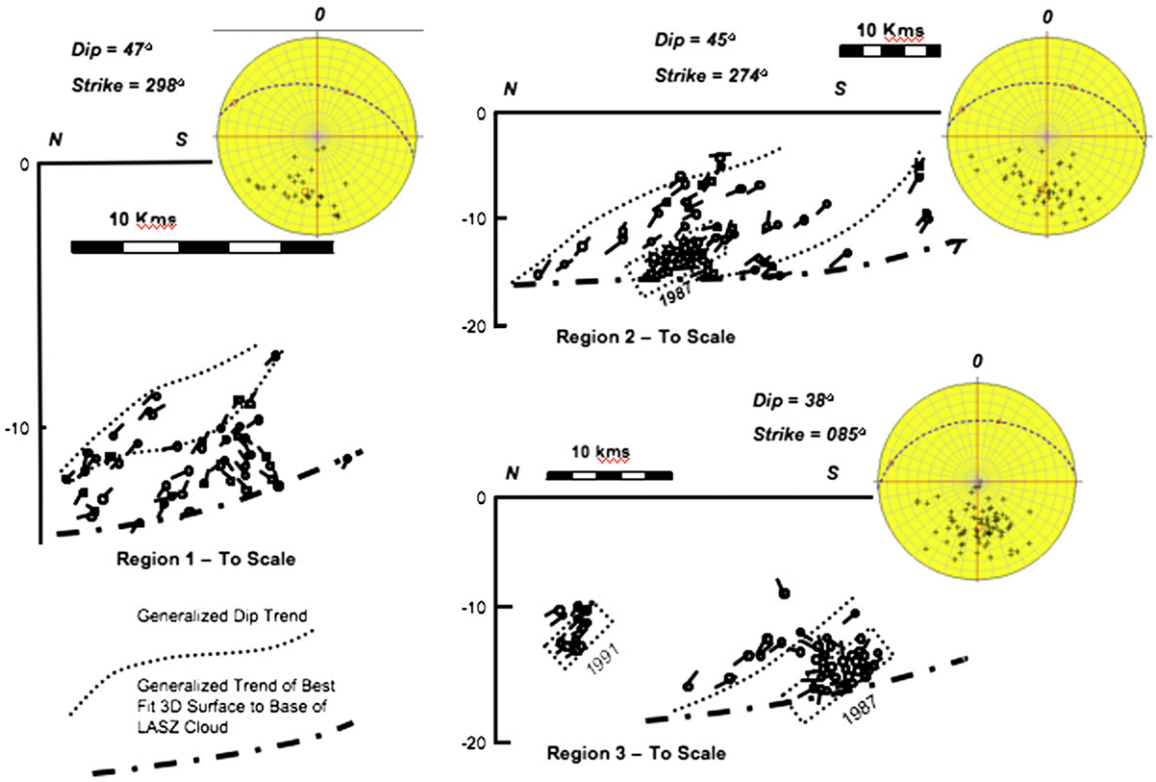

Fig. 4. Earthquake slip planes from regions 1–3 of Fig. 2 are projected onto north–south vertical profiles showing the internal geometry of the Los Angeles Seismic Zone earthquake "cloud". Only reverse fault data are shown (see Sections 2.3 and 3.2). Note that there are two geometric parameters for data; the average strike and dip of the slip planes forming the cloud given by the stereo-nets for each region and the strike and dip of the base of the cloud.

earthquake, aftershocks delineated a southwest-dipping fault that we will analyze.

The slip planes in Figs. 2 and 4 form prominent zones of background seismicity. Some display near continuous, low-magnitude activity, suggesting fault creep (e.g. Dolan et al., 1995) or diffuse strain associated with folding. An important large seismogenic region is an east–west zone of background seismicity that extends southward from the Transverse Ranges to Santa Monica Bay and includes the San Fernando, Northridge and Whittier earthquakes as well as the Elysian Park fold thrust belt of Hauksson and Saldivar (1989). The southern boundary includes the Los Angeles Basin (Fig. 1) and is named here the Los Angeles Seismic Zone (LASZ, Fig. 2).

2.3.2. *Interpretation of earthquake data – method*

The connection between the earthquake and structural data is the assumption that finite strain given by the structural data is the cumulative product of infinitesimal strains of which brittle failure, represented by the seismicity, is an unknown but presumably significant component.

Slip planes are determined and interpreted in a three step process:

Step 1: Hypocenter locations and focal mechanism solutions are determined, quality controls are applied and the earthquake data are sorted using QuakeView and the method of Seeber and Armbruster (1995) (Fig. 5).

For this study, all earthquakes of $M \geq 1.5$ were examined. Focal mechanisms are interpreted as slip planes and grouped into assemblages characterized by kinematic (strike, dip, rake) and spatial distribution. When grouped in this manner coherent spatial assemblages of slip planes emerge.

Step 2: Data from step 1 were imported into Geosec 3D and the earthquake slip planes displayed in 3D permitting the user to construct kinematic surfaces by connecting those slip planes that may

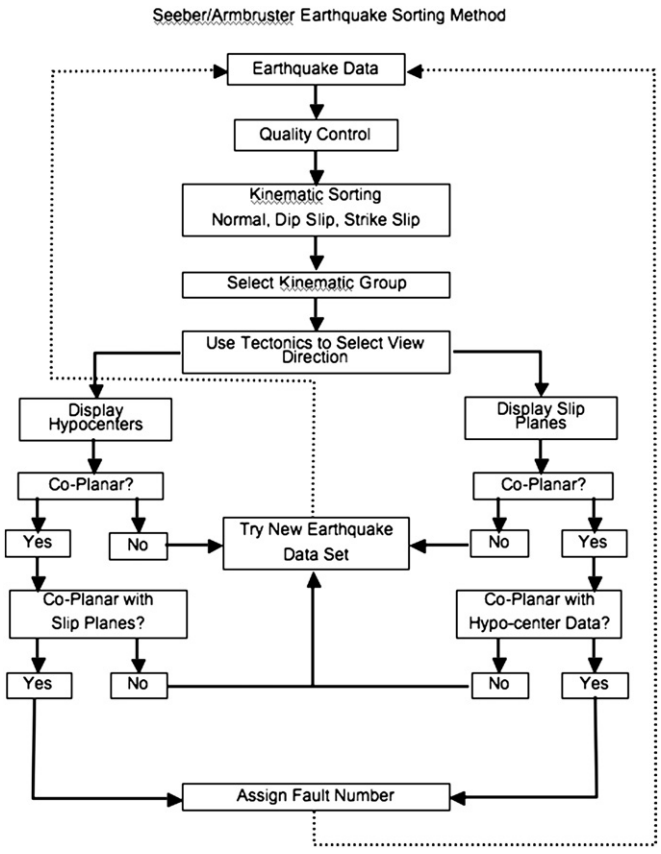

Fig. 5. Schematic illustrating the process used by Seeber and Armbruster (1995) for sorting earthquake slip planes into related structural and kinematic assemblages.

either lie on the boundaries of a cloud or else are better fit by a plane.

We recognize three types of slip plane data assemblages: *clouds*, *clusters* and *surfaces*.

1. *Clouds* consist of diffusely distributed slip planes forming an assemblage with small aspect ratios, are visible at 10+ km scale, contain parallel planes, and have well-defined boundaries (Fig. 4).
2. *Surfaces* are slip planes assemblages with large aspect ratios and parallel to sub-parallel slip planes. Surfaces occupy the 3–10 km length scale (Fig. 6).
3. *Clusters* are groups of slip planes resulting from persistent seismic activity localized in a relatively small volume (generally a few cubic kilometer).

Clusters are rare (e.g. the Whittier Narrows earthquake) and not well understood by us. We do not consider them further. The cloud and surface slip planes are sub-parallel to each other and to either the boundaries of the cloud or to a best-fit surface. Clouds have both internal and external order. Internal slip plane order is view dependent (e.g. as in viewing a cornfield where the rows can only be seen from certain directions), with slip plane orientations varying smoothly and coherently (e.g. Fig. 4). External slip plane order is represented by the surfaces bounding the seismogenic volume.

"Surface" assemblages are interpreted to illuminate faults with narrow "damage zones". Although we identify earthquake "Surface" assemblages that we interpret as fold associated, they parallel the fold geometry (i.e. forelimb, backlimb, etc.) and thus do not appear to be axial surfaces as suggested by Shaw and Suppe (1994) but rather sliding surfaces of the type found by Keunen and De Sitter (1938).

About 4000 quality-selected focal mechanisms were sorted to yield 3004 slip planes that yielded 19 distinct seismogenic assemblages. Of these, 13 are surfaces and six are clouds. Five assemblages both intersected the study region and were visible at the study scale. The assemblages are grouped temporally as well as spatially. The shortest time interval represented is 1 month, the longest is 23 years. The surfaces have undulating shapes while the clouds tend to be lensoidal cylinders and are the largest "objects".

Step 3: The earthquake data surfaces are compared to known structural surfaces. Positive or negative spatial correlation between the two data sets is used to test the interpretations. Elements that might cause false negative correlation between the data sets are:

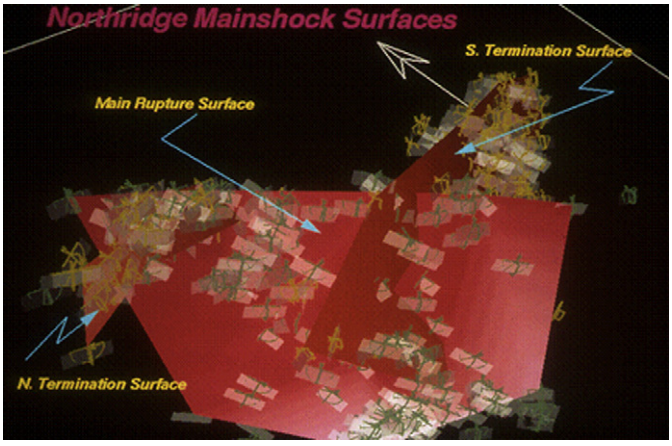

Fig. 6. 3D view of earthquake slip plane assemblages of main-shock rupture and Termination surfaces of the 1994 Northridge earthquake. View is down and towards the northeast. White arrow indicates north. Slip planes (semi transparent rectangles) are 500 m long (see Fig. 2 for location of this data set).

1. Earthquake data:
   a. Systematic location error.
   b. Systematic focal mechanism error.
   c. Misinterpretation of slip planes.
2. Structural data:
   a. Non-unique interpretation.
   b. Resolution problem due to sparse data (e.g. fold missing due to lack of critical dip data).

Once these factors are evaluated, the structural and earthquake data are reconciled by trial and error by choosing either permissible variation of the seismic velocity field parameters to change hypocenter locations or an alternate structural interpretation.

3. A 3D structural transect through the Eastern Transverse Ranges area using seismo-tectonic imaging

3.1. Regional tectonics of the Transverse Ranges

The Transverse Ranges are controlled by a system of east–west striking thrust faults intersecting the northwest striking San Andreas right-lateral transform. The mountain belt occurs at a major restraining bend in the transform boundary, the "Big Bend", that produces transpression. The Neogene evolution of the Transverse Ranges involves a transition from an extensional to a contractional regime and a large clockwise rotation.

Inverted basins in the Western Transverse Ranges indicate a change from an extensional to contractional regime about 5 my ago (Clark et al., 1991). Paleomagnetic measurements in the same area indicate 90° of clockwise rotation since at least the mid Miocene (Kamerling and Luyendyke, 1979). Both extension and rotation can be accounted for by rifting of the Transverse Ranges from the Peninsular Ranges in early Miocene (Kamerling and Luyendyke, 1979; Crouch and Suppe, 1993). The northward and clockwise motion of this upper crustal block was accommodated by shallow-dipping normal detachment faults with very large displacements (Bohannon and Geist, 1998; Crouch and Suppe, 1993; Nicholson et al., 1994). Clockwise rotation may be continuing in the current contractional regime (Luyendyk et al., 1980; Molnar and Gibson, 1994; Donnellan et al., 1993).

Current transpressional strain in the Transverse Ranges is partitioned (Mount and Suppe, 1987) with right-lateral motion primarily on the San Andreas Fault, while north–south shortening is primarily on a relatively broad system of east–west-trending thrust faults, both west and east of the San Andreas Fault. Thrust faults are responsible for many of the damaging earthquakes in the Transverse Ranges. Regionally continuous ramps are proposed as potential sources of very large earthquakes beneath the Western Transverse Ranges, including beneath Los Angeles basin (Yeats, 1981; Namson and Davis, 1988; Davis et al., 1989; Davis and Namson, 1994; Hauksson and Saldivar, 1989; Shaw and Suppe, 1994; Dolan et al., 1995).

In addition to right-lateral and contractional components, a third component of the partitioned deformation system is left-lateral slip on northeast to east striking faults represented by earthquakes (Hauksson and Jones, 1991; Seeber and Armbruster, 1995) and by a regional system of steep faults marking the southern topographic front of the Transverse Ranges.

3.2. The study volume

This study examines a 25 km deep, 50 × 10 km swath oriented north–south from the Northridge area to the Los Angeles basin (Figs. 1 and 2). The region is normal to the east–west trend of the Transverse Ranges and samples from the hanging wall of the Santa

Susana thrust, across the San Fernando basin to the footwall of the Santa Monica Fault to the south. The northern portion of the volume includes parts of the 1994 Northridge aftershock zone. This seismicity illuminates the main-shock rupture, as well as the adjacent 1971 San Fernando rupture to the east.

According to main-shock (Wald et al., 1996; Hudnut et al., 1996) and aftershock data (Hauksson et al., 1995 and Fig. 2), the Northridge rupture strikes WNW, dips at about 45° to the SSW with a strike length of about 18 km. The rupture was blind, initiating at a depth of about 20 km and extending upwards to a depth of about 7.5 km. Motion was primarily reverse dip–slip with a small right-lateral component. The rupture is cut off up dip at the intersection with the north dipping Santa Susana thrust fault. Davis and Namson (1994) suggest that the 1994 rupture occurred on the Pico Fault, a blind thrust interpreted from structural data. A problem with this and other correlations (e.g. Wald et al., 1996; Hudnut et al., 1996) is the mismatch between the east–west strike of structures in the San Fernando basin area (e.g. see Dibblee, 1982) and the WNW strike of the 1994 rupture.

The Los Angeles Seismic Zone, a prominent but markedly different seismic zone, is sampled by the southern portion of the study volume (Figs. 2 and 7). This zone has a minimum length of about 100 km and includes the northern part of the Los Angeles basin. The 20 years of seismicity on the Los Angeles Seismic Zone used in our study consists of temporally and spatially diffuse "background" seismicity made up of primarily EW striking, north dipping slip planes with predominant thrust motion. Most of the earthquakes in the Los Angeles basin belong to this assemblage.

The recognition of the Los Angeles Seismic Zone as a thrust system arises from the observation that although strike slip and normal earthquake slip planes occur in the Los Angeles Seismic Zone volume as well as below it, the reverse solutions uniquely form a cloud with a well-defined basal surface (Figs. 4 and 7). This observation is in agreement with Hauksson and Saldivar (1989) and Hauksson (1990), who note that at the Transverse Range/Coastal Range transition reverse fault solutions are restricted to the upper part of the crust.

The Los Angeles Seismic Zone includes the 1987 Whittier earthquake whose kinematics and location are consistent with the rest of the seismicity in this zone. Our data suggest that the Los Angeles Seismic Zone illuminates a major north dipping thrust system underlying the Los Angeles metropolitan area. Its southern tip corresponds to the Santa Monica thrust shown in the sections of Fig. 8.

Independent evidence for the Los Angeles Seismic Zone from earthquake tomography and deep reflection data (the LARSE line, Fig. 7) image a north dipping low velocity layer beneath the San Gabriel Mountains interpreted by Ryberg and Fuis (1998) as a young master decollement. A prominent reflector extending from this layer intersects and forms a lower bound to the 1987 Whittier Narrows earthquake which is at the base of the LASZ (Fig. 4) of which one focal plane is parallel to the reflector, thus tying to our map of the Los Angeles Seismic Zone.

3.3. Tectonic analysis

3.3.1. Selection of a deformation model for the Transverse Ranges

The deformed state sections (Fig. 8) are modified from four unpublished sections constructed by Davis and Namson (1996, personal communication) from a combination of well and outcrop data. Consistency with a flexural flow model is shown by spatially abrupt changes in dip directions reflecting angular bend folds. Use of the flexural flow deformation model permits application of the geometric rules of angular bend folding and faulting (e.g. Woodward et al., 1985; Groshong, 2006) to section construction and restoration. The 20 km wavelength of the largest folds wavelengths is interpreted to mean that these structures involve the entire upper crust.

3.3.2. Orientation of displacement field

The most recent deformation in the Transverse range is north–south contraction (e.g. Hill, 1982; Mount and Suppe, 1987; Wald et al., 1996). Thus, to a first-order, displacement vectors are strike-normal making the four strike-normal cross sections vector-parallel and thus allowing restoration. Restoration was done

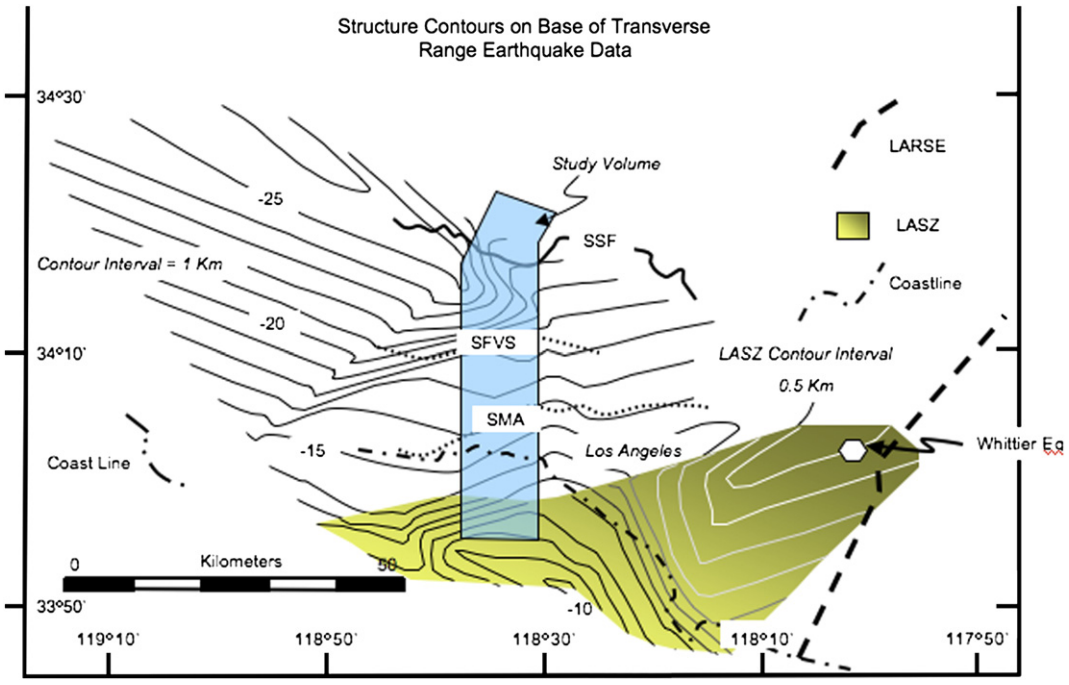

Fig. 7. Structure contour map of base of all reverse slip earthquake data used in study. SFVS = San Fernando Valley Synclinorium, SMA = Santa Monica Anticlinorium, SSF = surface trace of Santa Susana Fault, LASZ = Los Angeles Seismic Zone, LARSE line location from Ryberg and Fuis (1998).

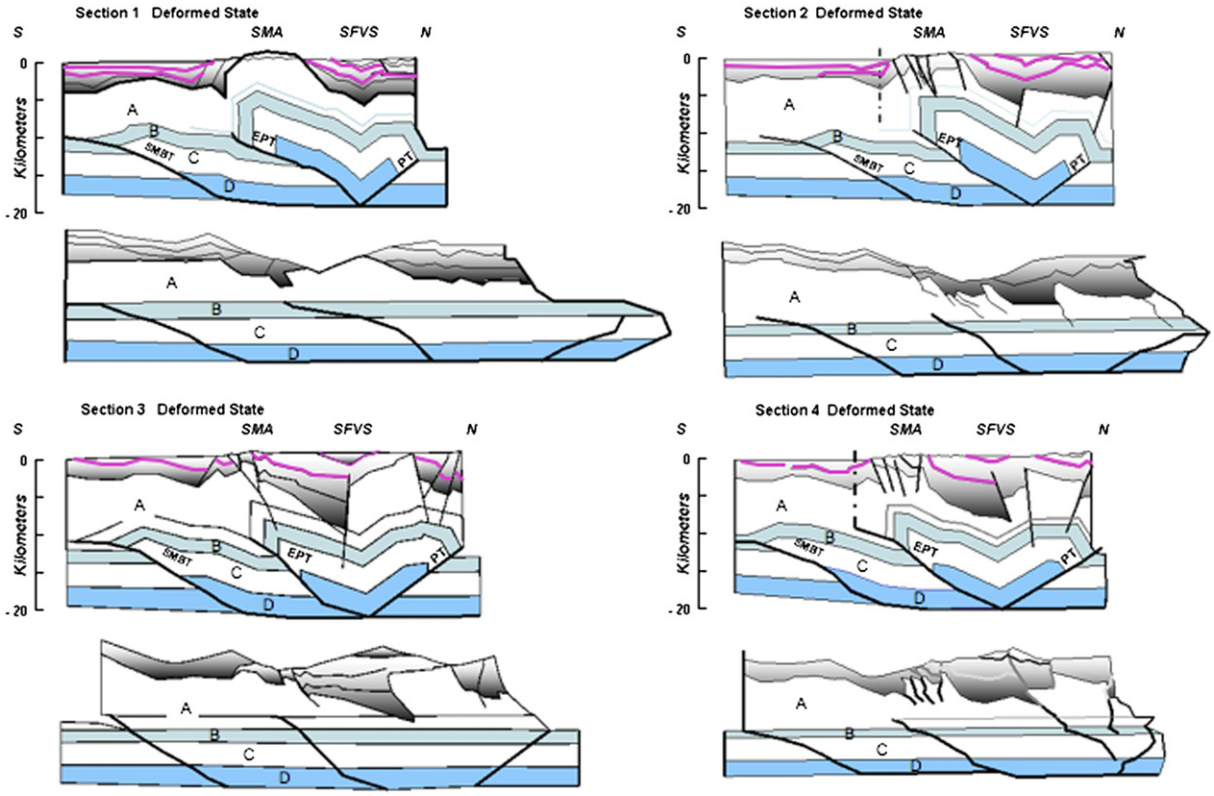

Fig. 8. Deformed and restored state cross sections across study area. See Fig. 1 for locations. Construction horizons = top and bottom of Monterey Fm. Colored lines give general location of construction horizons. Projection horizons for crystalline "basement" = top of unit A or light line above B. SMA = Santa Monica Anticlinorium; SFVS = San Fernando Valley Synclinorium; SMBT = Santa Monica Bay thrust; EPT = Elysian Park thrust; PT = Pico thrust. Shaded Units = Sediments; Solid Colors = Basement. Basement units A–D are only for construction purposes.

with GeoSec 2D using the standard kinematic rules related to angular fault-related folds and fault systems (e.g. Woodward et al., 1985; Groshong, 2006).

The Malibu Coast–Santa Monica–Hollywood–Raymond–Cucamonga (MSHRC) fault system, the southern boundary of the Transverse Range, creates issues for the restorations because there is at least local left-lateral motion with vertical surface fault traces (e.g. Campbell and Yerkes, 1976; Dibblee, 1982). However, Seeber and Armbruster (1995) (Fig. 3) show that removing this system from consideration only creates small errors, so we follow this practice.

3.3.3. 3D transect construction

The 2D deformed state sections (Fig. 8) served as input for 3D Geosec where the 3D interpretation was constructed using hinge lines, dip domain boundaries and fault cutoffs as constraining lines. The 3D interpretation consists of internal construction surfaces (units A–C of Fig. 8; NB: these are kinematic not "bedding" surfaces) and boundary surfaces located by construction (e.g. the Pico thrust, Elysian Park thrust, etc.). This interpretation was used to check for lateral compatibility in both the deformed and undeformed state.

3.4. Upper crustal structure

3.4.1. Thick-skinned vs. thin-skinned

The fundamental nature of Transverse Range tectonics is controversial (e.g. Yeats, 1995). Our analysis indicates that the Transverse Ranges are thin-skinned (Figs. 4, 6 and 7). The interpretation of thin-skinned behavior is supported by:

1. The gradual northward increase in depth of reverse fault seismicity towards the more internal parts of the Transverse Range (Fig. 7).
2. Slip planes' dips for thrust earthquakes tend to decrease with depth, i.e. they are listric (Fig. 9).
3. The north dipping low velocity layer and reflectors found by Ryberg and Fuis (1998) congruent with the base of reverse slip seismicity of this study.

3.4.2. First-order structure

The upper crustal structure is reflected by the first-order fold geometry of the Transverse Ranges (e.g. the Santa Monica

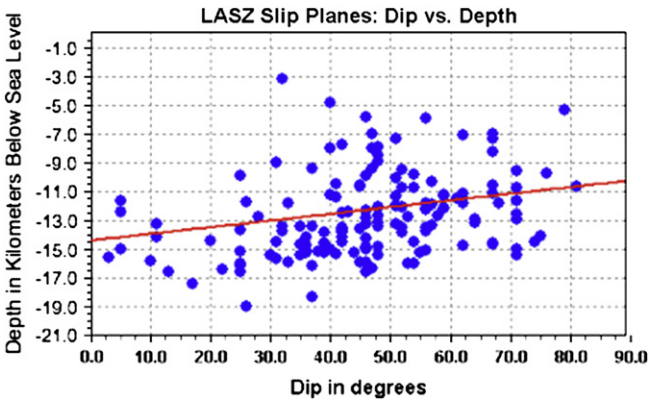

Fig. 9. Plot of dip vs. depth for the reverse slip focal planes of Los Angeles Seismic Zone.

Mountain Anticlinorium/San Fernando Valley Synclinorium, etc.). The top of the Monterey formation and the basal Monterey unconformity are used to construct the cross sections and to provide datum surfaces for restorations. These surfaces control the "deformation stratigraphy" (units A–D in Fig. 8) used to visualize structural geometry.

While surface and well data are effective for constraining the upper 3–5 km of the four cross sections, the earthquake distribution data best define the geometry of the basal detachment (Figs. 4, 7, 9 and 10). Consequently, the lower boundary of the reverse slip seismicity locates the basal detachment.

3.5. 3D tectonic analysis

The study area is interpreted to contain three thrusts that branch from the basal detachment (Fig. 8). The Pico and Elysian Park faults are a linked synthetic/antithetic pair of fault-propagation anticlines and define the limbs of the San Fernando Valley Synclinorium. The most external thrust, for which we propose the name Santa Monica Bay thrust (corresponding to the leading edge of the Los Angles Seismic zone), has a related fault-bend anticline (Fig. 8: sections 3 and 4) that loses displacement to the east becoming a fault-propagation fold (section 1: Fig. 8).

The solution we chose for the Pico and Elysian Park thrusts in which they share a common branch line is representative of a class of solutions in which the axial surface of the San Fernando Valley Synclinorium coalesces progressively higher in the section. The location of the coalescence point is controlled by the width of the flat between the Elysian Park and Pico thrusts. We lack sufficient data to locate the exact depth of the coalescence point and therefore the exact location of the branch line(s). We have chosen the single branch line solution that places it on the sole fault, but note that the 28% decrease in shortening between sections 3 and 4 (see Fig. 8 and Table 2) suggests that the coalescence point may not be on the flat for section 4 as the additional flat would decrease the difference in shortening between the sections.

3.5.1. Restored state

Our restoration (Fig. 8) only removes displacement on first-order structures, the Santa Monica Bay, Elysian Park and Pico thrusts and not the small amount of shortening represented by the normal fault reactivation. The normal faults are interpreted to have reactivated to accommodate the strains produced during the formation of the first-order structures and show as small reverse faults in the restored sections. This partial validation of the sections provides:

(1) A test of compatibility between hanging wall and footwall templates.
(2) Estimates of shortening values.
(3) Information on the nature and distribution of global simple shear implied by the deformed state solution.

3.5.2. Hanging wall/footwall compatibility

The restorations show that compatibility between hanging wall/footwall templates is good with some minor misfits appearing in sections 1 and 3. The "smooth" fault trajectories of the Santa Monica Bay and Elysian Park thrusts suggest formation by faulting of the "basement" (deformation units A–D, Fig. 8), producing the fault-related folding shown. The irregular trajectories of the Pico and Elysian Park faults in section 4 indicate that either folding may have preceded faulting of the basement (i.e. a "break thrust", Willis,

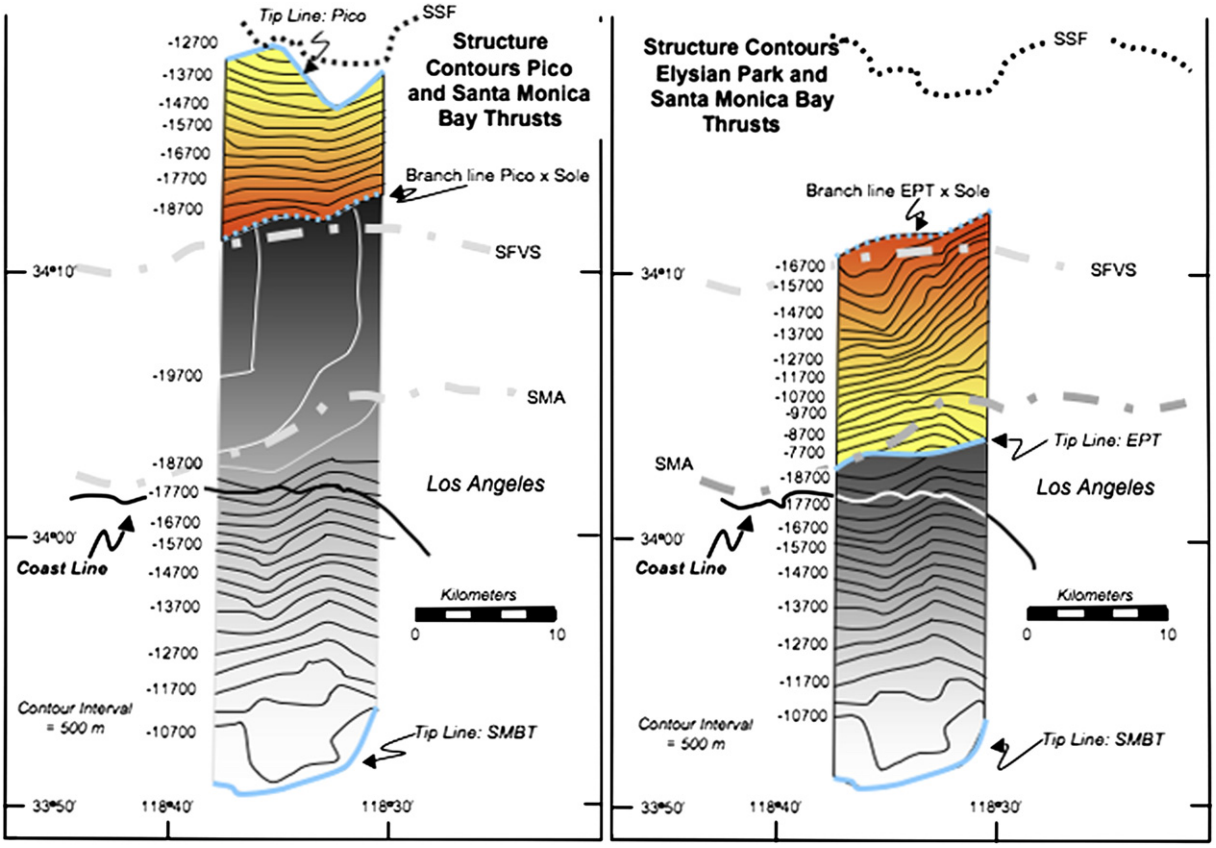

Fig. 10. Structure contour maps of Santa Monica Bay (SMB), Elysian Park (EPT) and Pico thrusts. SFVS = San Fernando Valley Synclinorium, SMA = Santa Monica Anticlinorium, SSF = surface trace of Santa Susana Fault. Location of sole fault is from earthquake data. All splays (e.g. EPT, Pico) and tip of SMB located by construction from surface data. Note that the EPT and Pico thrusts share a common branch line.

Table 2
Data from deformed and restored state sections of Fig. 8 used to calculate variation and amount of shortening for study volume

Section	1	2	3	4
Deformed state (km)	51.6	49.3	52	48.1
Restored state (km)	71.4	65.8	67.7	59.5
Shortening (%)	28	25	24	20
Rate (mm/yr)	8.6	7.2	6.8	4.9

The difference in shortening rates between lines 3 and 4 reflects the decision to use the same branch line (Pico × Elysian Park) location for all interpretations.

1894) or incorrect deformed state geometry (Geiser, 1988). Evidence for the sole fault is indicated by the consistent shear sense reversal and increase in the displacement gradient shown by deformation units A and B in all sections.

3.5.3. Shortening rates and section validation

An independent test of the validity of the transect sections (Fig. 8) in terms of bed-length is to compare the shortening rate calculated using the shortening of our interpretations to the current (geodetic) Transverse Range shortening rate of 13 ± 2 mm/yr given by Fiegl et al. (1993). Because our sections do not include the entire Transverse Range, the calculated shortening rate should be less than that measured by Fiegl et al. (1993). Bulk shortening values are calculated from the restored and deformed lengths of the sections (Fig. 8 and Table 2). Shortening decreases from east to west.

To calculate average shortening rates, the shortening magnitudes are divided by the age for Transverse Range deformation initiation. Age estimates vary from 5 (Wright, 1991; Blake, 1991) to 2.3 my (e.g. Davis and Namson, 1994). The shortest estimate of 2.3 my gives the greatest shortening rate. We use this value. Table 2 shows that the calculated shortening rates meet the requirement of being less than the current.

4. Structural and kinematic analysis of seismogenic structures of the Los Angeles area using seismo-tectonic imaging

This section discusses the structural and kinematic interpretation of the earthquake data in terms of two independent data sets: geology and reflection seismology. The purpose is to assess the validity of our method for analyzing background and aftershock seismicity by comparing the results with those derived from different phenomena.

4.1. Relationship of 1994 main-shock rupture to geologic structure

Two sets of reverse slip aftershock slip planes (Groups 1 and 2) are closely associated in space and kinematics with the main-shock rupture. The data define three best-fit surfaces and are subdivided into two assemblages (Fig. 11).

4.1.1. Assemblage 1 – Main Rupture Surface (MRS)

The Group 1 slip planes are fit by a "surface" assemblage striking 330–325 and dipping at ≈55° W. The best-fit surface essentially

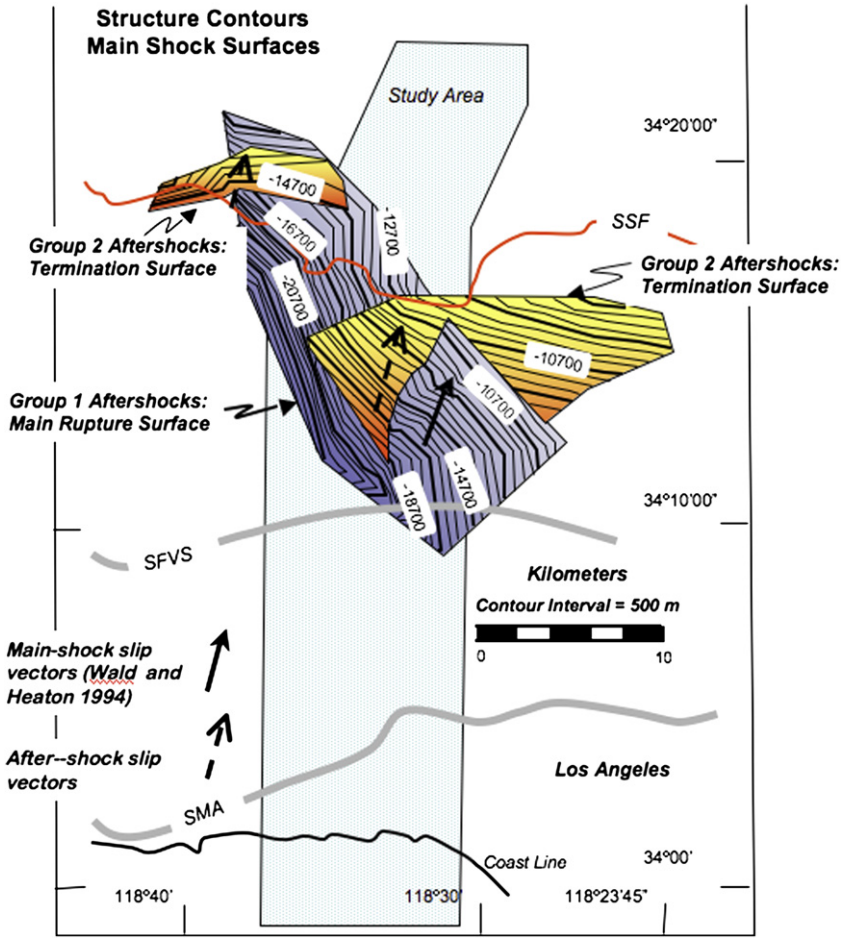

Fig. 11. Structure contour maps of Main Rupture Surface (MRS) and Termination surfaces imaged from aftershock data shown in Fig. 6. Note positions of surfaces relative to the structural salient indicated by the surface trace of the Santa Susana Fault (SSF). Aftershock and main-shock slip vectors identical. SFVS = San Fernando Valley Synclinorium; SMA = Santa Monica Anticlinorium.

coincides in size, position and kinematics with the fault that ruptured in the main-shock (e.g. Wald and Heaton, 1994).

4.1.2. Assemblage 2 – lateral "Termination" surfaces

The Group 2 slip planes are fit by two en-echelon "surface" assemblages striking about 285 and dipping south at 45–50°. These surfaces mark lateral extensions of the MRS as defined by assemblage 1. Although the surfaces were not part of the Main Rupture event, slip on the MRS caused loading of these surfaces, which was relieved during the aftershock period. Therefore, they are considered to be an important kinematic element of the Northridge earthquake. As kinematic compatibility requires, the intersections of the aftershock defined surfaces are sub-parallel to the near vertical main-shock slip vectors (e.g. Wald and Heaton, 1994) as well as the predominant aftershock slip vectors of assemblages 1 and 2 (Fig. 11).

The three best-fit surfaces suggest a sigmoidal form (Fig. 11) with the MRS centrally located in the Santa Susana Fault salient. The location and attitude of the southern surface of assemblage 2 (Fig. 11) closely agrees with that of the Pico Fault located by section construction (Fig. 12). We take this to indicate that although the Pico played a role in the Northridge earthquake, the main-shock rupture surface was not the South–Southwest-dipping Pico as suggested by Davis and Namson (1994) and Hauksson et al. (1995). The northern surface of assemblage 2 is outside the study region but is tentatively assigned to the Oak Ridge thrust system (Yeats et al., 1994). We suggest that the assemblage 2 surfaces represent the termination of the main-shock rupture.

We interpret the MRS and its terminations as a variant on the *secondary transverse tear fault* model of Dahlstrom (1970). Although Dahlstrom uses the term "tear fault" to describe the model (Fig. 13), the connecting fault only becomes a tear once the hanging walls move onto the footwall flats. Until this occurs, motion on the connecting fault is dominantly dip–slip and parallel to the fault intersections. In our interpretation, this is the current stage of deformation. An additional departure from Dahlstrom's model is that we have no evidence that the transverse fault postdates the thrusts. It is entirely possible that the fault is a result of reactivation of a pre-existing structure as suggested by the MRS strike, which parallels the trend of the Northern Peninsular ranges.

Accordingly in our model the 1994 main rupture occurred on a transverse fault linking the Pico and Oak Ridge thrust systems with some of the slip transferred to the two EW trending thrust faults. Thus, the Northridge earthquake occurred on a secondary fault in relation to the thrusts that dominate the structural architecture and represent the greatest potential earthquake hazard.

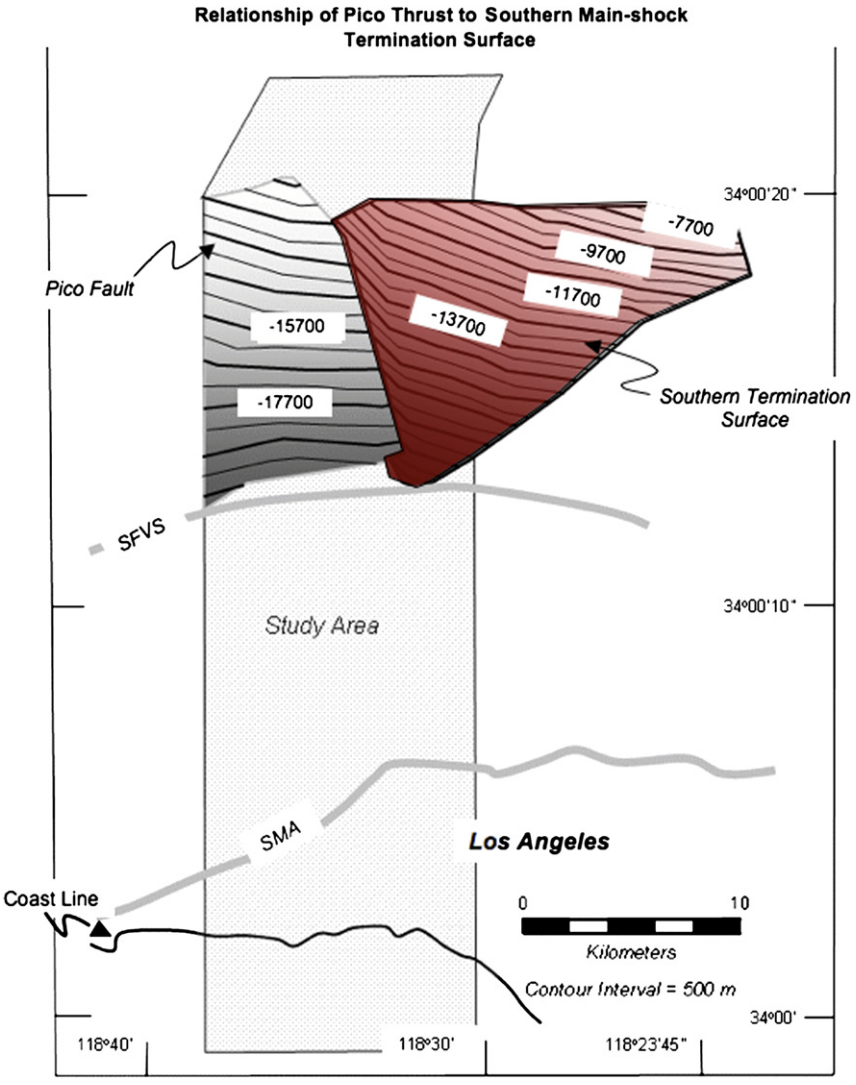

Fig. 12. Structure contours on southern main-shock "Termination" surface (shaded red) and Pico thrust (shaded white). Congruence suggests that the Pico was one of the "Termination" surfaces rather than the main-shock surface as suggested by Davis and Namson (1994).

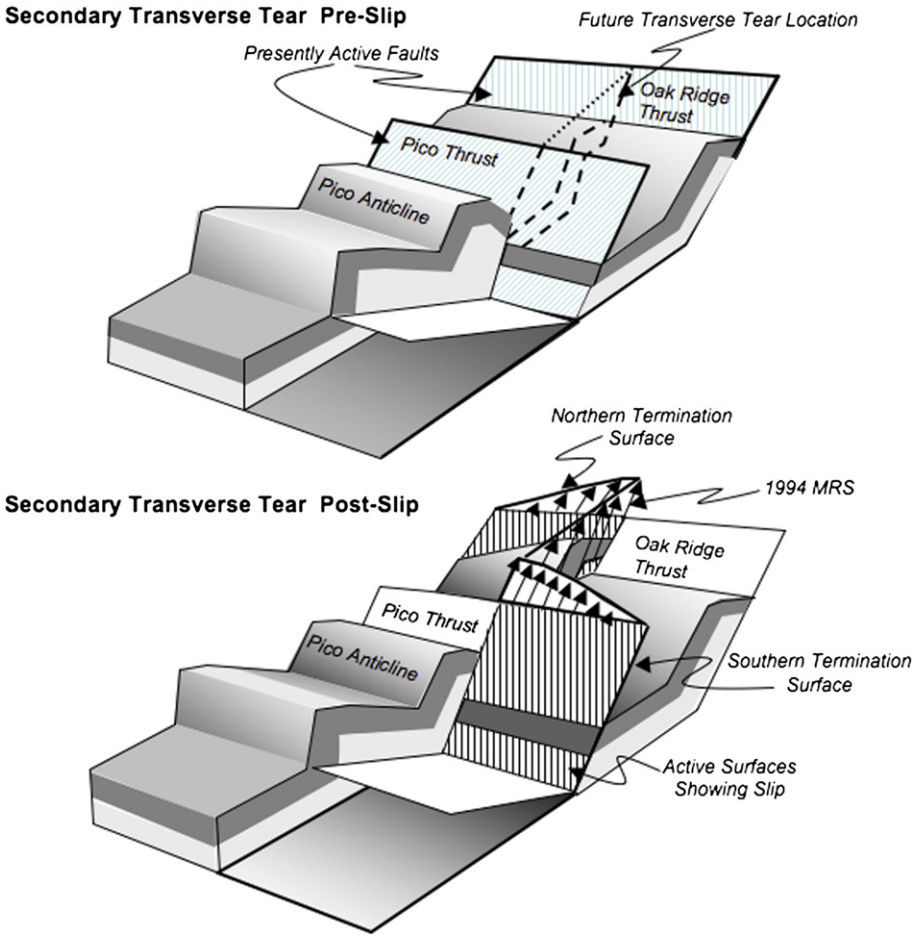

Fig. 13. Schematic diagram of the geometry and kinematics of proposed secondary transverse tear model (after Dahlstrom, 1970) for the Northridge earthquake slip surfaces. Note presence of cross-strike folding.

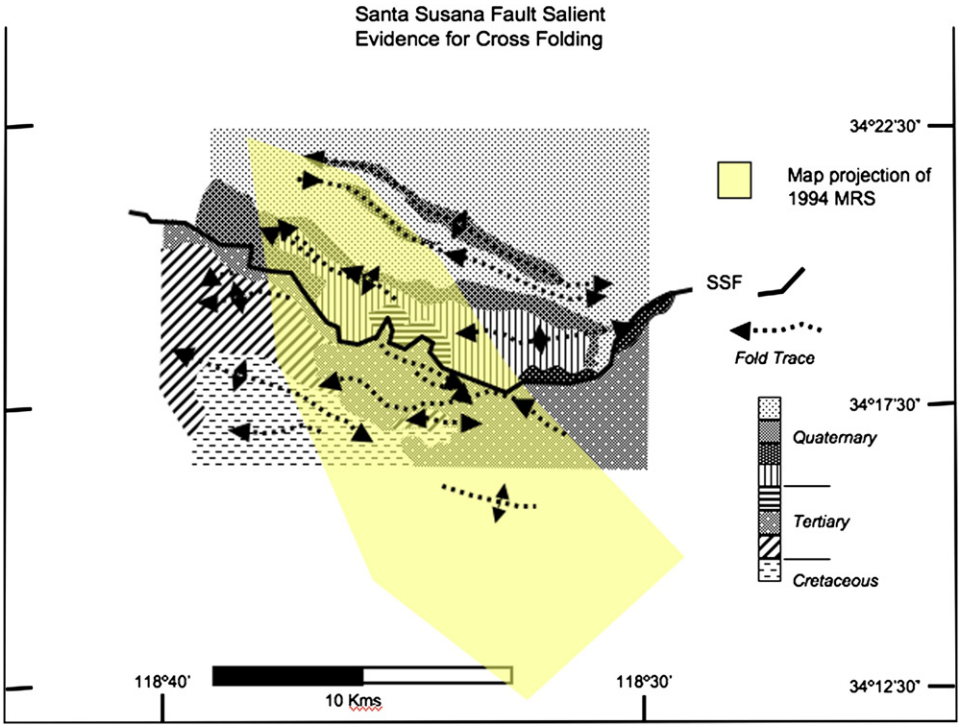

Fig. 14. Geologic data in vicinity of Santa Susana Fault (SSF) salient. These data show pattern of plunge reversals and periclinal folding in the region underlain by the cross-strike Main Rupture Surface. Data compiled from Dibblee Foundation maps DF 33, 36 and 38.

4.2. Inferred kinematics of the Northridge rupture

Although our interpretation of the MRS (Figs. 11 and 13) is based on seismicity it can also be tied to the surface geology by recognizing that the deep earthquake structure is reflected by regional-scale map structures. Fig. 11 shows that the MRS lies immediately below the Santa Susana Fault salient. The kinematics of the MRS (Fig. 13) predicts that accumulated slip on the MRS should create a cross-strike anticline. Examination of the regional structure (Fig. 14) reveals that the axis of the salient roughly coincides with a region of fold plunge reversal i.e. on the west side of the salient, folds tend to plunge west whereas on the east side they tend to plunge east. In addition the NW trending part of the trace of the Santa Susana Fault west of the MRS is sub-parallel to the strike of the MRS. This geometry is consistent with a NW trending antiformal structure folding the trace of the SSF. Recognition of this transfer fault (MRS) of the Pico and Oak Ridge systems requires both structural and seismicity data. Further, the model shows that the high-angle dip geometry for the MRS is consistent with a thin-skinned solution, so a thick-skinned interpretation favored by Yeats (1995), Hauksson et al. (1995) and Huftile et al. (1995) is not necessary.

4.3. The Los Angeles Seismic Zone (LASZ)

The Los Angeles Seismic Zone (Fig. 7) has been continuously active through the period covered by the earthquake data considered in this study (1973–1993) and can be labeled as "background" seismicity distinguishing it from the more intense but highly time-dependent aftershock activity in the Northridge and San Fernando areas. The Los Angeles Seismic Zone appears as a "cloud" of hypocenters south of the frontal faults of the Transverse Ranges (Fig. 7 and Hauksson and Saldivar, 1989, Fig. 6). It is parallel to and south of the Raymond Hills, Santa Monica, Dume Fault system and can be traced for almost 100 km from Point Dume to Pasadena (Figs. 1 and 7). This represents the minimum extent of the zone as the structural trends continue to the west where earthquake data are rare due to the paucity of stations. The interpretation as a single large structure is consistent with the other large regional structures (Figs. 1 and 7) and also with the uniformity of the kinematics and internal structure indicated by the earthquake slip planes (Fig. 4). The latter suggest a major EW striking thrust system verging to the south superimposed on a NW trending system of right-lateral faults (also Hauksson, 1990; Hauksson and Saldivar, 1989).

The basal surface fitted to this cloud begins at the approximate top of the most external ramp (the Santa Monica Bay Fault; Figs. 8 and 10) required by Davis and Namson (1994) interpretation for the Santa Monica Anticlinorium. North of the coastline, the strike of the Los Angeles Seismic Zone is sub-parallel to the trend of the hinge surface trace of the Santa Monica Anticlinorium (Fig. 7). Southeast of the study area, a strike change from EW to NNW in the basal surface occurs near the coast and is on strike with a major N-S zone of structural discontinuity reflected in interrupted fold and fault trends on the east side of the Ventura Basin and the shift to NNW striking folds and faults of the Los Angeles basin and the Elysian Park and the Torrance–Wilmington fold/thrust belts (compare Figs. 1 and 7). These correlations suggest:

- The frontal ramp (Santa Monica Bay Fault) required by Davis and Namson (1994) interpretation exists and therefore supports the validity of the first-order structure they propose.

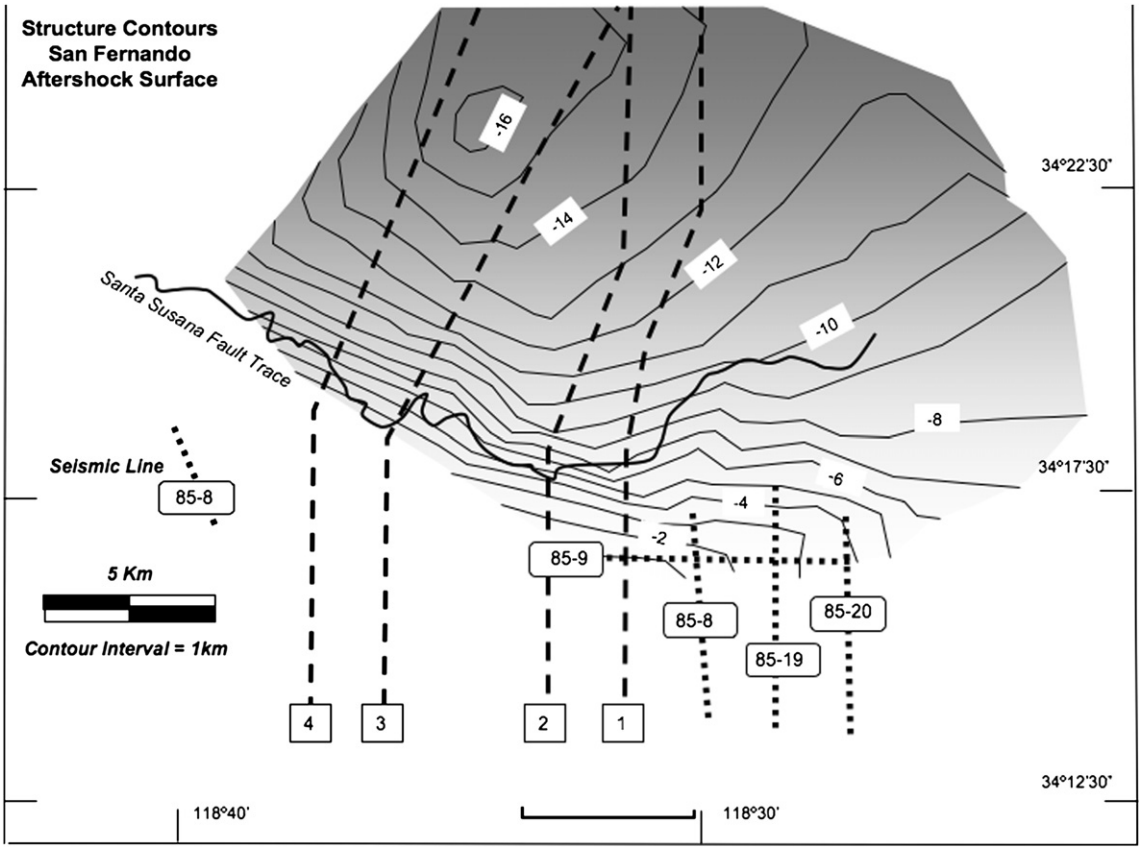

Fig. 15. Structure contours on aftershock data from the 1971 San Fernando Valley earthquake. Note that the basal surface geometry is listric, i.e. flattens with depth; 1–4, indicate location of cross sections shown in Fig. 8A, B, C, D. The dotted lines give location and number of the seismic sections shown in Fig. 16.

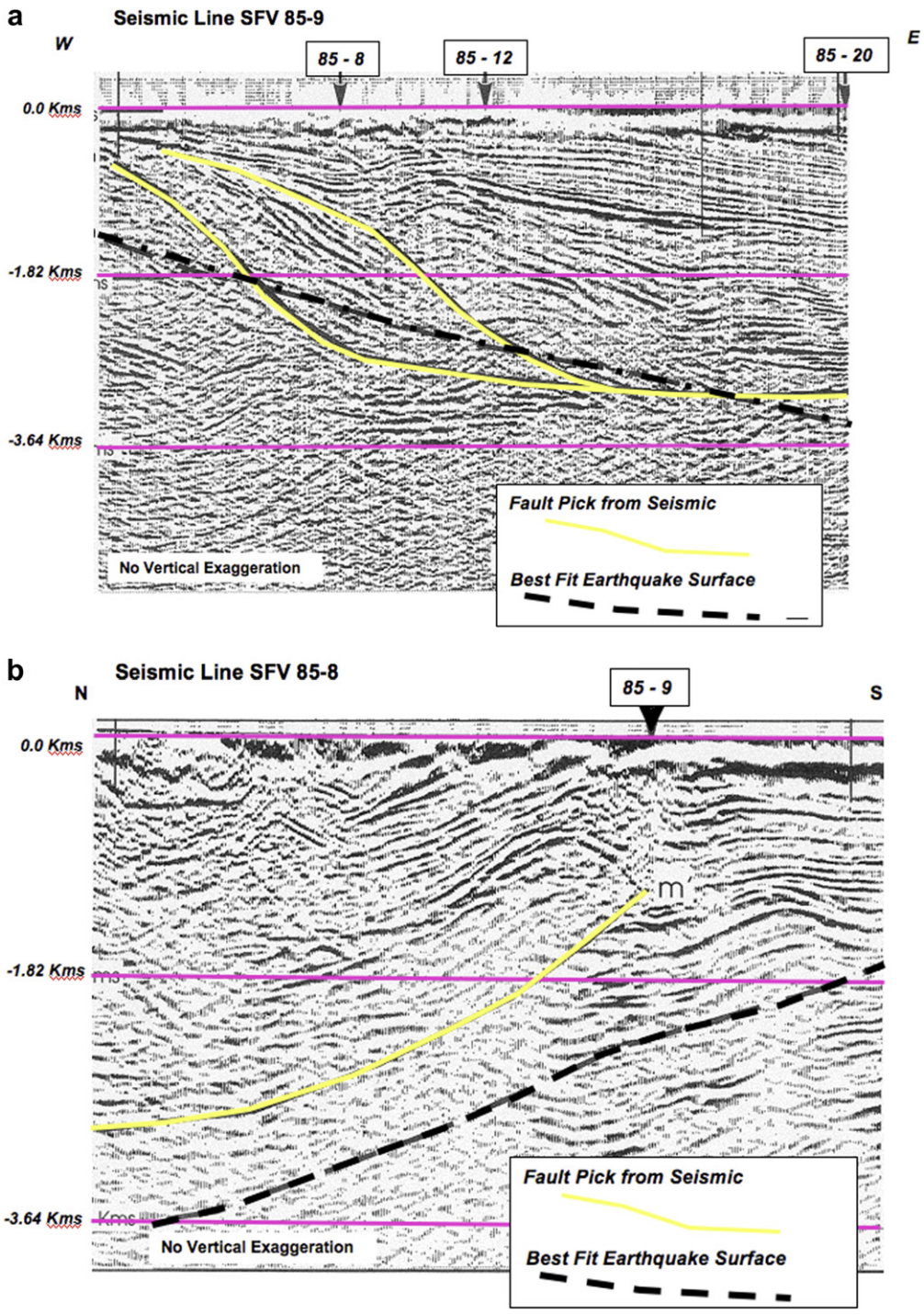

Fig. 16. San Fernando Valley seismic sections showing degree of fit between faulting imaged by seismic and base of Santa Fernando Valley Earthquake cloud. Line of best-fit earthquake surface in seismic is line of intersection between best-fit earthquake surface to San Fernando Earthquake Surface and seismic line. See Fig. 15 for section locations; 16a = strike line; 16b–d = dip lines from west to east. Seismic data depth converted using GeoSec 2D with a uniform velocity field of 3640 m/s.

- The Santa Monica Anticlinorium is the current Mountain Front, but with southward progradation of the thrust wedge, it is being abandoned for the LASZ and the SMBF.

Earthquake slip plane data show three characteristics of the Los Angeles Seismic Zone:

- An EW thrust system exists beneath Santa Monica Bay, which becomes a more SE striking system beneath the northern LA basin.
- The Elysian Park and the Torrance–Wilmington fold/thrust belts change from NW trend to an ENE trend as the Los Angeles Seismic Zone is approached (e.g. Hauksson, 1990 and Figs. 1 and 7).
- There are co-existing decoupled strike slip and thrust systems (Hauksson, 1990).

Slip plane dips tend to decrease with depth (Figs. 7 and 9), while the zone as a whole has a wedge shape with the base deepening to the north (Fig. 7). Although antithetic, south-dipping slip planes

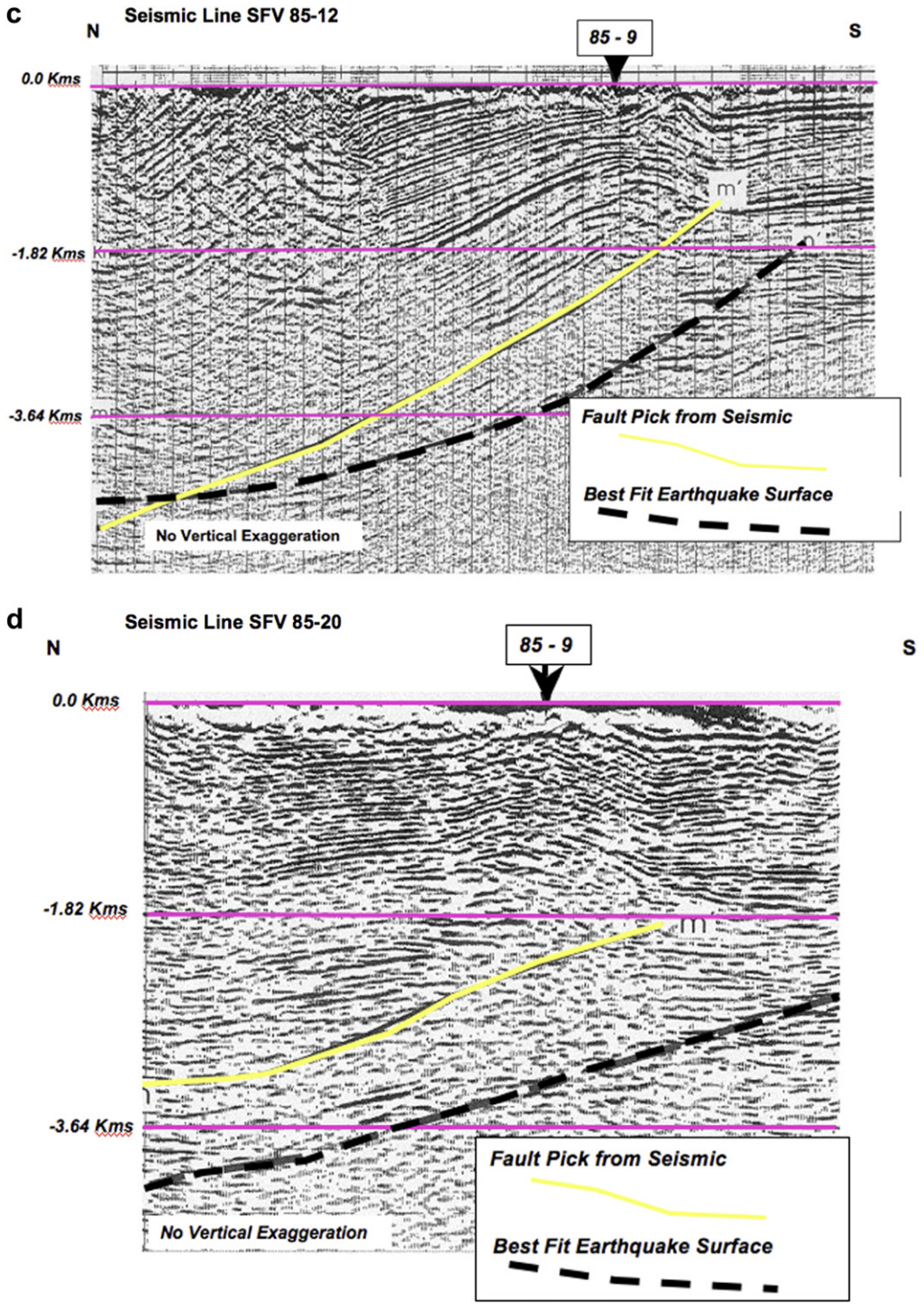

Fig. 16. (*continued*).

occur, synthetic orientations suggesting duplex-like structures dominate (Fig. 4). Well-resolved examples of shallow thrusts within the wedge are: [1] the 1987 M6.1 Whittier rupture displayed as a 30° dipping and ~5 km wide thrust patch (Fig. 4; also Hauksson and Jones, 1991; Davis et al., 1989) and [2] a pair of imbricate thrusts in Santa Monica Bay (Hauksson and Saldivar, 1989). We include the Wilshire fault, described by Hummon et al. (1994) as a north dipping blind thrust with a large right-lateral component, as a member of the Los Angeles Seismic Zone fault system. Finally, as previously noted, Ryberg and Fuis's (1998) work on the LARSE line is consistent with our interpretation of the Los Angeles Seismic Zone.

4.4. San Fernando Valley earthquake (1971) and seismic reflection data

Aftershock data from the 1971 San Fernando Valley earthquake form a "cloud" in the vicinity of the Santa Susana Fault. We refer to the cloud's basal surface as the San Fernando Aftershock Surface (Fig. 15). We infer it to be a forward-breaking imbricate of the Santa Susana Fault propagating into the sedimentary fill of the San Fernando Valley implying that the Santa Susana Fault has abandoned or is abandoning the strand presently mapped as the Santa Susana Fault.

The reflection data consist of three dip-parallel vertical seismic reflection profiles tied by a strike-parallel vertical seismic reflection profile (Fig. 15) and image an eastward plunging growth thrust. Fig. 16 shows that the San Fernando Aftershock Surface agrees well in both orientation and depth with the sole fault interpreted from the seismic reflection data.

In addition to the close fit to the thrust fault seen in the seismic reflection data, the earthquake surface has two additional attributes suggesting that it represents a forward-breaking splay of the Santa Susana Fault.

- It has a listric geometry (Fig. 15).
- The sequence and structural location of faulting with respect to the SSF suggest footwall collapse, typical of forward-breaking thrust fault systems.

4.4.1. Relation of San Fernando aftershock surface to the Northridge rupture

Fig. 17 superposes the structure contour maps for the Northridge Main Rupture Surface and its terminations with that for the San Fernando Aftershock Surface and shows that the surface is continuous and above the Northridge rupture surfaces. This supports Hauksson et al. (1995) and Wald et al. (1996) proposal that movement on the Northridge was capped by the Santa Susana Fault and did not reactivate any of the 1971 earthquake faults. The strike of the structure contours changes from ENE to WNW along the trace of the Main Rupture Surface, consistent with the kinematic model that we propose for the Northridge earthquake (e.g. Figs. 13 and 14). Finally we note that although our data support the general notion proposed by Yeats and Huftile (1995) that both the footwall and hanging wall of the Santa Susana Fault system have been folded by an underlying fault, our data do not support their interpretation that the uplift occurred on the WNW trending continuation of the Oak Ridge thrust. Rather the uplift is the result of activity of a NNW striking "secondary transverse tear" linking the EW trending Pico and Oak Ridge thrusts.

5. Summary and conclusions

We have integrated three independent three-dimensional data sets (structural, earthquake seismology and seismic reflection data) to analyze the tectonics of a section of the southern California Transverse Range. The main structural results are:

- The 1994 Northridge rupture occurred on a transverse fault linking the Pico and Oak Ridge thrust systems. The rupture effectively terminated at the intersection between the transverse faults and the thrusts.
- The Los Angeles Seismic Zone is a zone of thrusting associated with the development of a new mountain front forming south of the present one represented by the Santa Monica Anticline. The thrust is rooted on a mid-crustal ramp forming beneath the LA basin.
- We find three types of earthquake distributions:
  [1] Clouds of earthquakes associated with distributed deformation of internal deformation fields produced by folding and/or faulting.

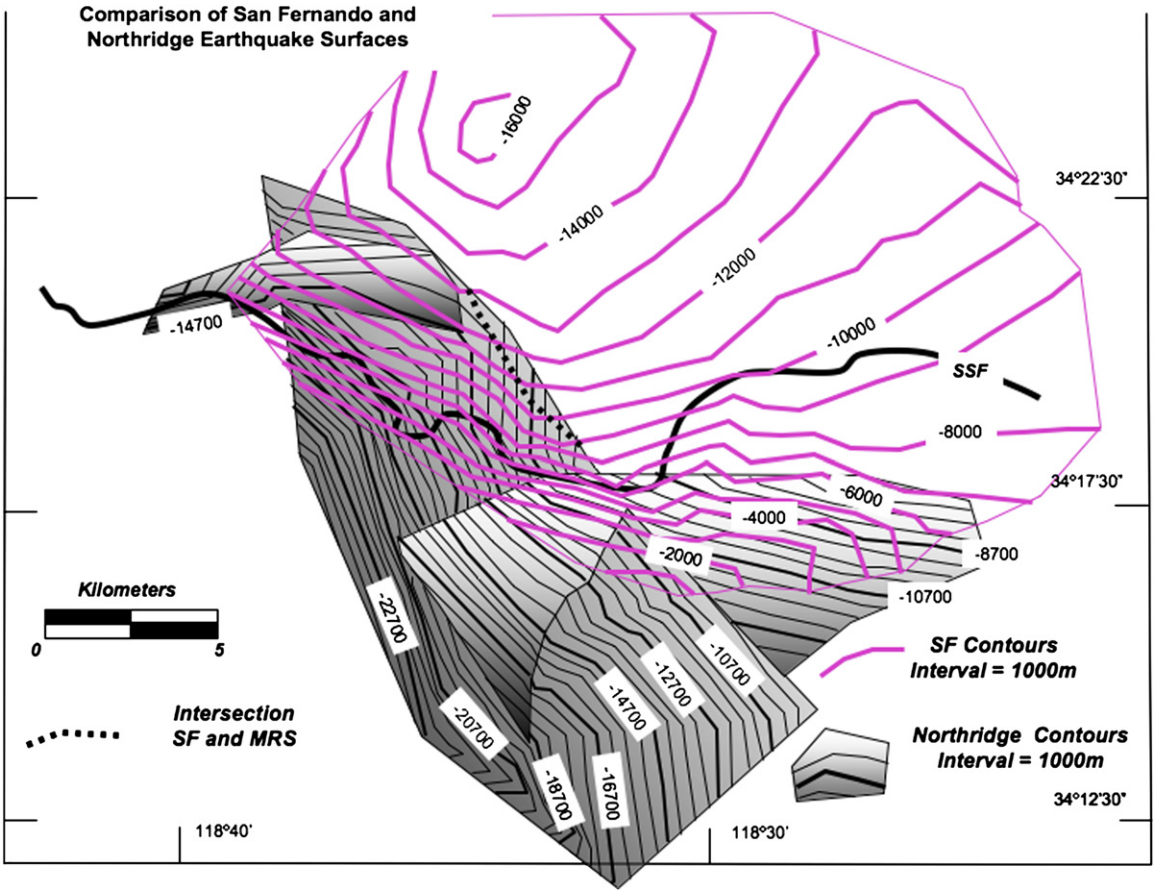

Fig. 17. Structure contours for the Northridge Main Rupture (MRS) and San Fernando Valley (SF) earthquake surfaces. Note the change in strike of the SF surface above the MRS. SSF = trace of Santa Susana Fault.

[2] Surfaces associated with individual regions of limited slip which may be either boundaries of individual fault blocks of limited displacement or fold sliding surfaces.
[3] Clusters: these are regions of localized activity whose origin is not understood.

Our use and integration of independent data sets provide a means of achieving greater confidence for:

- Distinguishing between tectonically active and inactive structures.
- Discriminating earthquake assemblages in terms of their structural significance.
- Imaging structures in terrane opaque to reflection seismology.
- Establishing structural and kinematic relationships that are otherwise difficult to determine.

Regarding the tectonics of the Transverse Ranges, the data support both a ramp/flat geometry for basement as well as evidence for deep, high-angle faults and suggest a model for compatibility between these faults. It is also consistent with the inference that flexural flow is a reasonable representation of the first-order behavior of the earth's crust in the Transverse Ranges. We interpret the Los Angeles Seismic Zone as the basal detachment of a part of the Transverse Ranges. This detachment is now forming a new Mountain front propagating into the Los Angeles basin. This zone has a minimum strike length $>$100 km. If this interpretation is correct then the possibility exists for a major shallow (10–15 km) blind thrust earthquake directly beneath Los Angeles. We note that the proposed fault is an order of magnitude larger than other potential earthquake faults previously recognized.

Acknowledgements

We want to thank Jay Namson and Thom Davis for the generous contribution of their geological data and knowledge of southern California geology. This information was vital for the interpretation and imaging of the Transverse Range structure. We also express our appreciation to Chris Sorlien for his help in the tectonic analysis and critical reading of the manuscript, to John Armbruster and Jim Geiser for their help with developing the earthquake related software, to Alan Morris and Bill Dunn for exhaustive and invaluable manuscript reviews and to the Princeton Structural Geology group for their assistance in obtaining the seismic reflection data. We gratefully acknowledge Silicon Graphics for their equipment loans to this project. Financial and software support for this work was provided by Cogniseis Development and the following grants: NSF: EAR 94-16222; USGS: 1434-HQ-97GR-03016; USGS: 1434-HQ-95-G-2576; SCRC: USC P.O. 569934, scope A.

References

Blake, G.H., 1991. Review of the Neogene biostratigraphy and stratigraphy of the Los Angeles Basin and implications for basin evolution. In: Biddle, K.T. (Ed.), Active Margin Basins. AAPG Memoir, vol. 52. American Association of Petroleum Geologists, Tulsa, pp. 135–184.

Bohannon, R.G., Geist, E.L., 1998. Upper crustal structure and Neogene tectonic development of the California continental borderland. Geological Society of America Bulletin 110, 779–800.

Campbell, R.H., Yerkes, R.F., 1976. Cenozoic evolution of the Los Angeles basin area – relationship to plate tectonics. In: Howell, D.G. (Ed.), Aspects of the Geological History of the California Borderland: Pacific Section, vol. 24. American Association of Petroleum Geologists Misc. Publication, pp. 541–558.

Clark, D.H., Hall, N.T., Hamilton, D.H., Heck, R.G., 1991. Structural analysis of late Neogene deformation in the central offshore Santa Maria Basin, California. Journal of Geophysical Research 96 (B4), 6435–6457.

Crouch, J.K., Suppe, J., 1993. Late Cenozoic tectonic evolution of the Los Angeles basin and inner California borderland: a model for core complex-like crustal extension. Geological Society of America Bulletin 105 (11), 1415–1434.

Dahlstrom, C.D.A., 1970. Structural geology in the eastern margin of the Canadian Rocky Mountains. Bulletin of Canadian Petroleum Geology 18 (3), 332–406.

Davis, T., Namson, J.S., 1994. A balanced cross section analysis of the 1994 Northridge earthquake and thrust fault seismic hazards in southern California. Nature 372, 167–169.

Davis, T.L., Namson, J., Yerkes, R.F., 1989. A cross section of the Los Angeles area: seismically active fold and thrust belt, the 1987 Whittier Narrows earthquake and earthquake hazard. Journal of Geophysical Research 94 (B7), 9644–9664.

Dibblee, T.W., 1982. Geology of the Santa Monica Mountains and Simi Hills, Southern California. In: Fife, D.L., Minch, J.A. (Eds.), Geology and Mineral Wealth of the California Transverse Ranges. Annual Symposium and Guidebook, vol. 10. South Coast Geological Society, pp. 94–130.

Dolan, J.F., Sieh, K.E., Rockwell, T.K., Yeats, R.S., Shaw, J., Suppe, J., Huftile, G.J., Gath, E.M., 1995. Prospects for larger or more frequent earthquakes in the Los Angeles metropolitan region. Science 267, 199–205.

Donnellan, A., Hager, B.H., King, R.W., Herring, T.A., 1993. Geodetic measurement of deformation in the Ventura Basin region, southern California. Journal of Geophysical Research 98, 21727–21739.

Fiegl, K.L., et al., 1993. Space geodetic measurements of crustal deformation in central and southern California. Journal of Geophysical Research 98, 21677–21712.

Geiser, P.A., 1970. Deformation of the Bloomsburg Formation, Cacapon Mountain Anticline, Hancock, Maryland. Ph.D. thesis, Johns Hopkins University, Baltimore.

Geiser, P.A., 1988. The role of kinematics in the construction and analysis of geological cross sections in deformed terranes. In: Mitra, G., Wojtal, S. (Eds.), Geometry's and Mechanisms of Thrusting with Special Reference to the Appalachians. Geological Society of America, Special Paper, vol. 222.

Geiser, J., Geiser, P.A., Kligfield, R., Ratliff, R., Rowan, M., 1988. New applications of computer based section construction: strain analysis, local balancing and subsurface fault prediction. Mountain Geologist 25 (2), 47–59.

Groshong Jr., R.H., 2006. 3-D Structural Geology, second ed. Springer-Verlag, Heidelberg, 400 pp.

Hauksson, E., 1990. Earthquakes, faulting and stress in the Los Angeles Basin. Journal of Geophysical Research 95 (B10), 15365–15394.

Hauksson, E., Saldivar, G.V., 1989. Seismicity and active compressional tectonics in Santa Monica Bay, Southern California. Journal of Geophysical Research 96 (B5), 8143–8165.

Hauksson, E., Jones, L.M., 1991. The 1988 and 1990 Upland earthquakes: left-lateral faulting adjacent to the Central Transverse Ranges. Journal of Geophysical Research 96 (B5), 8143–8165.

Hauksson, E., Jones, L.M., Hutton, K., 1995. The 1994 Northridge earthquake sequence in California: seismological and tectonic aspects. Journal of Geophysical Research 100 (B7), 12335–12355.

Hill, M.L., 1982. Anomalous trends of the San Andreas Fault in the Transverse Ranges, California. In: Fife, D.L., Minch, J.A. (Eds.), Geology and Mineral Wealth of the California Transverse Ranges. Annual Symposium and Guidebook, No. 10. South Coast Geological Society, pp. 367–369.

Hudnut, K.W., Shen, Z., Murray, M., McClusky, S., King, R., Herring, T., Hager, B., Feng, Y., Donnellan, A., Bock, Y., 1996. Co-seismic displacements of the 1994 Northridge, California, earthquake. Bulletin of the Seismological Society of America 86 (1B), S19–S36.

Hummon, C., Schneider, C.L., Yeats, R.S., Dolan, J.F., Sieh, K.E., Huftile, G.J., 1994. Wilshire fault: earthquakes in Hollywood? Geology 22 (4), 291–294.

Huftile, G.H., Tsutsumi, H., Schneider, C.L., Yeats, R., 1995. Geologic Evidence for Thick-skinned Deformation in the Western Transverse Ranges, California, Thrust Ramps and Detachment Faults in the Western Transverse Ranges. SCEC Workshop, January 22–24, 1995, Institute for Crustal Studies, UCSB, Abstract: 12.

Kamerling, M.J., Luyendyke, B.P., 1979. Tectonic rotations of the Santa Monica Mountains region, western Transverse Ranges, California. Journal of Geophysical Research 90 (B14), 12485–12502.

Keunen, P.H., De Sitter, L.U., 1938. Experimental investigation into the mechanism of folding. Leidse Geologische Mededelingen 10, 217–240.

Luyendyk, B.P., Kammerling, M.J., Terres, R.R., 1980. Geometric model for Neogene crustal rotations in southern California. Geological Society of America Bulletin 91, 211–217.

Marshak, S., Geiser, P.A., Alvarez, W., Engelder, T., 1982. Mesoscopic fault array of the northern Apennine fold belt, Italy: a case of conjugate shear by pressure solution. Geological Society of America Bulletin 93 (10), 1013–1022.

Molnar, P., Gibson, J.M., 1994. Very long baseline interferometer and active rotations of crustal blocks in the western Transverse Ranges, California. Geological Society of America Bulletin 106, 594–606.

Mount, V.S., Suppe, J., 1987. State of stress near the San Andreas fault: implication for wrench tectonics. Geology 15, 1143–1146.

Namson, J., Davis, T.L., 1988. Structural transect of the western Transverse Ranges, California: implications for lithospheric kinematics and seismic risk evaluation. Geology 16, 675–679.

Nicholson, C., Sorlien, C.C., Atwater, T., Crowell, J.C., Luyendyk, B.P., 1994. Microplate capture, rotation of the Western Transverse Ranges and initiation of the San Andreas transform as a low-angle fault system. Geology 22, 491–495.

Ramberg, H., 1961. Relationship between concentric longitudinal strain and concentric shearing strain during folding of homogeneous sheets of rocks. American Journal of Science 259, 382–390.

Ramsay, J.G., 1967. Folding and Fracturing of Rocks. McGraw Hill Book Co.

Rutledge, J.T., Fairbanks, T.D., Albright, J.N., Boade, R.R., Dangerfield, J., Landa, G.H., 1994. Reservoir Microseismicity at the Ekofisk Oil Field. Eurock'94, pp. 589–595.

Ryberg, T., Fuis, G.S., 1998. The San Gabriel Mountains bright reflective zone: possible evidence of mid-crustal thrust faulting. In: Klemperer, S.I., Mooney, W.D. (Eds.), Deep Seismic Profiling of the Continents, I: General Results and New Methods. Tectonophysics, vol. 286, pp. 31–46.

Seeber, L., Armbruster, J.G., 1995. The San Andreas Fault system through the Transverse Ranges as illuminated by earthquakes. Journal of Geophysical Research 100 (5), 8285–8310.

Seeber, L., Armbruster, J.G., 2000. Earthquakes as beacons of stress change. Nature 407, 69–72.

Shaw, J.H., Suppe, J., 1994. Active faulting and growth folding in the eastern Santa Barbara Channel, California. Geological Society of America Bulletin 106, 607–626.

Suppe, J., 1983. Geometry and kinematics of fault bend folding. American Journal of Science 283, 684–721.

Wald, D.J., Heaton, T.H., 1994. A Dislocation Model of the 1994 Northridge, California, Earthquake Determined from Strong Ground Motions. United States Geological Survey Open-file Report, pp. 94–278.

Wald, D.J., Heaton, T.H., Hudnut, K.W., 1996. The slip history of the 1994 Northridge, California, Earthquake determined from strong-motion, teleseismic, GPS, and leveling data. Bulletin of the Seismological Society of America 86 (1B), S37–S49.

Willis, B., 1894. Mechanics of Appalachian Structure, 13th Annual Report, United States Geological Survey, 1891–92, pp. 213–291.

Woodward, N.B., Boyer, S.E., Suppe, J., 1985. An Outline of Balanced Sections. In: Studies in Geology, second ed., vol. 11. University of Tennessee, Department of Geological Sciences, Knoxville.

Wright, T.L., 1991. Structural geology and tectonic evolution in the Los Angeles Basin, California. In: Biddle, K.T. (Ed.), Active Margin Basins. American Association of Petroleum Geologists Memoir, vol. 52. American Association of Petroleum Geologists, Tulsa, pp. 35–135.

Yeats, R.S., Huftile, G.J., Stiff, L.T., 1994. Late Cenozoic Tectonics of the East Ventura Basin, Transverse Ranges, California. American Association of Petroleum Geologists Bulletin 78 (7), 1040–1074.

Yeats, R.S., Huftile, G.J., 1995. The Oak Ridge fault system and the 1994 Northridge earthquake. Nature 373, 418–420.

Yeats, R.S., 1995. Thin-skinned vs. Thick-skinned Interpretation of Seismogenic Reverse Faults, Thrust Ramps and Detachment Faults in the Western Transverse Ranges, Southern California Earthquake Center Workshop, University of California Santa Barbara, Abstracts, pp. 29–30.

Yeats, R.S., 1981. Quaternary flake tectonics of the California Transverse Ranges. Geology 9, 16–20.